Lighting protection methods for wind turbine blades: an alternative approach.

MUCSI, V., AYUB, A.S., MUHAMMAD-SUKKI, F., ZULKIPLI, M., MUHTAZARUDDIN, M.N., SAUDI, A.S.M. and ARDILA-REY, J.A.

2020

Lightning Protection Methods for Wind Turbine Blades: An Alternative Approach

**Viktor Mucsi [1], Ahmad Syahrir Ayub [1,*] , Firdaus Muhammad-Sukki [1,*] ,
Muhammad Zulkipli [2] , Mohd Nabil Muhtazaruddin [3] , Ahmad Shakir Mohd Saudi [4,*] and
Jorge Alfredo Ardila-Rey [5]**

[1] School of Engineering, Robert Gordon University, The Sir Ian Wood Building, Riverside East, Garthdee Road,
     AB10 7GJ Aberdeen, UK; v.mucsi@rgu.ac.uk
[2] Faculty of Engineering Technology, Universiti Tun Hussein Onn Malaysia, Pagoh Higher Education Hub,
     KM1, Jalan Panchor, Pagoh, Muar 84600 Johor, Malaysia; muhammad@uthm.edu.my
[3] Razak Faculty of Technology and Informatics, Universiti Teknologi Malaysia, Jalan Sultan Yahya Petra,
     Kuala Lumpur 54100, Malaysia; mohdnabil.kl@utm.my
[4] Universiti Kuala Lumpur-Institute of Medical Science Technology (UniKL MESTECH), A1-1, Jalan TKS 1,
     Taman Kajang Sentral, Kajang 43000, Selangor, Malaysia
[5] Department of Electrical Engineering, Universidad Técnica Federico Santa María, Santiago de Chile 8940000,
     Chile; jorge.ardila@usm.cl
*   Correspondence: a.ayub2@rgu.ac.uk (A.S.A.); f.b.muhammad-sukki@rgu.ac.uk (F.M.-S.);
     ahmadshakir@unikl.edu.my (A.S.M.S.)

Abstract: Lightning strikes happens in a fraction of time, where they can transfer huge amounts of charge and high currents in a single strike. The chances for a structure to be struck by lightning increases as the height increases; thus, tall structures are more prone to lightning. Despite the existing lightning protection systems available for wind turbine blades, there are still many cases reported due to the fact of damage caused by lightning strike. Owing to that, the present work introduces a new approach for a lightning protection system for wind turbine blades where preliminary investigations were done using Analysis Systems (ANSYS) Workbench. Two models were developed: one with a conventional type down conductor system and the other with a hybrid conductor system. The recorded findings have been compared and discussed, where it was found that the hybrid conductor system may provide alternative protection from lightning for wind turbine blades.

Keywords: lightning; lightning protection system; wind turbine blades; ANSYS workbench

1. Introduction

Windmills have been around for centuries, operating as grain grinders and water pumps. The concept and technology behind windmills have been adapted to generate electricity, which in its new form is now called wind turbines (i.e., wind energy). Wind energy generation is now becoming one of the largest contributors to renewable energy generation, where the recent demand for renewable energy has seen its increasing growth in use as well as in physical size. In other words, wind turbines are getting taller, in order to accommodate the demand, by capturing wind through a larger blade swept area and converting it into electricity. Owing to this, wind turbines are now more prone to lightning strikes due to the fact of their increased structural height.

There are approximately 2000 thunderstorms at any given minute and about 100 lightning strikes per second worldwide [1]. This creates great risk for tall structures, such as wind turbines, to be struck by lightning, where the average electric current from a lightning return stroke is 30 kA [1]. This massive flow of current can heat up the leader channel air to between 25,000 °C and 30,000 °C (around five

times the effective temperature of the sun) [1–3]. Lightning protection system (LPS) is composed of lightning receptor, down conductor, and grounding, and all elements must be well connected to pass the lightning current to Earth safely. Although wind turbines are installed with LPS, there are still cases where blades and whole turbines are destroyed due to the fact of lightning strikes. Considering the 20–25 year design life for wind turbine [3], it is worth safeguarding the turbines from lightning strikes, because the damage associated with it will cause the down time of the turbine operation, causing extra costs for maintenance and an shortage of electricity. This, therefore, may suggest a need for improving the existing lightning protection systems for wind turbine blades.

2. Lightning Discharges and Existing Lightning Protection Systems for Wind Turbine

Mechanism of Lightning Discharge

Lightning discharge from cloud to ground stems from a stepped leader initiated in a cloud and increases the electric field within its path. When a grounded object is in that electric field, it generates a leader towards the stepped leader, and it is called a connecting leader. If the downward moving leader has a negative charge, then the connecting leader is positive. If the downward leader is negative, then the connecting leader is positive [3].

As a stepped leader approaches ground level or the tip of the grounded structures, the electric field increases to such an extent that it discharges, and connecting leaders starts to propagate towards the downward leader in an attempt to connect, to equal the potential difference. Taller structures generate longer connecting leaders due to the field enhancement caused by the accumulation of positive charge on the structure [1,3,4].

The stepped leader channel is at cloud potential, approximately 50 MV [1,3–8] and with the final connecting jump, a near of ground potential travels along the channel in the direction of the cloud, which is called return stroke. The flow of charge generates a large current with an average peak of 30 kA [1,3] to 80 kA [1]. Due to the rapid generation of heat of around 30,000 K [1,3] in the channel, a pressure is created of 10 atm or above [3]. In some instances, new charges from the cloud forming another electrical discharge called dart leaders, creating subsequent return strokes with an average peak current of about 10–15 kA [1,3].

Most negative cloud-to-ground flashes contain more than one stroke, generally 3–4 [1] and, in major cases, the first stroke is usually 2–3 [3] times larger than the following subsequent strokes. On the other hand, occasionally in multiple stroke flashes there is at least one subsequent stroke which is greater than the first return stroke [3].

3. Wind Turbine Blades and Its Protection Methods

3.1. Wind Turbines and Blades

There are two main types of wind turbines on the market nowadays: vertical axis and horizontal axis turbines. Due to the lower efficiency, vertical axis turbines were not considered in this paper. Modern turbines are dominantly composed of horizontal axis models, since with rotor blade pitching, the speed of rotation and hence the power output can be controlled, and the blade aerodynamics can be optimized for maximum efficiency. In most cases, the three-blade model is used as it has the highest efficiency in ratio of the number of blades and their overall weight.

At blade design, the actual shapes are very similar within commercial turbines, although, slightly differs by each manufacturer for the best possible aerodynamics according to company preferences [9]. Common characteristics are the hollow design, to reduce weight and the turnable rotor blade tip to help overspeed limitation [10]. Modern blades generally made of Fiber-Reinforces Composites such as carbon fiber and glass fiber with a matrix material of polyester resins or epoxy resins.

Carbon fiber generally has good braking and elasticity characteristics, with stiffness not far from steel, although it is the most expensive material component among the possible choices. Also, in regards

to lightning protection, it requires special considerations due to the fact of its material properties which are similar to a semiconductor, creating issues with lightning attachment and flashovers on the surface of the blade.

Glass fiber, on the other hand, has lower ratings in almost all the characteristics mentioned before, but it is considerably cheaper, and it acts as an insulator. Manufacturers tend to use it with more expensive but high-quality epoxy resins to enhance the required physical properties of it [10,11]. Although, the blade is nonconductive, it still attracts lightning due to the fact of its height; therefore, lightning protection is necessary.

3.2. Lightning Protection in General

Lightning protection systems for wind turbines are based on International Electrotechnical Commission (IEC) IEC 61400-24. According to this standard, the lightning protection levels (LPLs) have been set in accordance with the probability of minimum and maximum expected lightning currents, I to IV. The maximum protection, LPL I levels should not be exceeded with a probability of 99% for negative flashes, meanwhile, for positive flashes it is below 10% [12]. The parameters for LPL II and III–IV are the reduced values of LPL I by 75% and 50%, respectively.

The rolling sphere method (RSM) was used to identify the locations of the air termination system on a given structure. The method assumes that there is a spherical region with a radius equal of the striking distance located around the tip of the oncoming lightning leader to a structure. Owing to that, the RSM method demonstrated on a wind turbine with 20 m radius (LPL I). This radius, r, is in relation to the peak current I of the first stroke. According to the IEEE, the equation is:

$$r = 10I^{0.65} \tag{1}$$

There are many different proposals regarding the calculations of the radius for the rolling sphere in relation with the peak current, but the suggested values for each protection level are set by the standards [7] where for each LPL and radius, there is a corresponding minimum peak current value which, against the protection level, it gives protection.

3.3. Protection Methods for Blades

There are four main types of lightning protection methods developed as recommended and outlined in IEC 61400-24 [7]. The methods are as follow:

(a)   receptors placed in the tip and an internal wire (i.e., conductor) is used to carry the current to the hub
(b)   metallic conductor placed around the edges to serve as termination and down conductor
(c)   metal mesh used on the side of the blade

Regardless of the methods, the main function [12–14] of the lightning protection on the blades is:

-   Successful attachment of the lightning strike to a designated or preferred air termination or down conductor system to conduct the current safety without damaging the blades;
-   Provide passage for the lightning current through sufficient cross-section conductors, diverters, and air terminators to earth. Preventing damage to the system and minimizing the high level magnetic and electric field due to high currents;
-   Minimizing the high level of voltages induced and observed inside and outside of the turbine.

With insulator-based materials blades, such as glass fiber composites, the conductors can be placed outside of the blade to divert lightning from the blade surface, also, can be placed inside, with air-terminations at specific point outside of the blade. When carbon fiber composites are used, a layer of conducting material is placed over it which can then carry the current to the blade root. With

both cases, sliding connectors are used to carry the current from the blade to the hub towards the ground [12–14].

For the earth termination and down conductors, it has to carry the lightning current safely to the ground where common materials are aluminum, steel, and copper. In general, air termination and for down conductor, the cross-section of at least 50 mm^2 is recommended [7,12–14].

3.4. Lightning Damage to Wind Turbines and Blades

According to many field observations and studies [15–18], wind turbines receive significant amounts of lightning attachments during their designed lifetime, mostly on rotor blades. The percentage distribution of damaged parts due to the lightning strike can be seen in Figure 3. The damages caused mostly from unsuccessful attachments on air terminations or from induced voltages from electric and electromagnetic fields. The highest percentage of damages occurred on the control system, although, on some cases, the damage were simple interruptions. Meanwhile the damage caused on blades are 11%, it often corresponds with severe damage. The damages associated with lightning are generally blade rupturing and burnout, wire melting, surface cracking and delamination, lightning receptor vaporization, and loss [19–25].

The most popular lightning protection model used nowadays for large turbines consist of an internal down conductor and metal receptors or air terminators penetrating the surface of the blade to serve as desired attachment points. These two systems are then connected together inside of the blade to carry the lightning current to earth. The receptors are installed at nearby the tip of the blade or placed at equal distance from each other alongside the blade from the root to the tip.

One of the main issues with this type of protection is that since the receptors are small compared to the blade planform area, it decreases the efficiency of the attachment of the lightning, causing damage on the surface of the blade [21–25].

Considering the distribution of the lightning attachment and damage along the blade, it can be seen that majority of the attachment occurs at the tip, and the percentage decreases as the distance increasing from the end of the blade. As it can be seen, around 60% of the total damage was located in the last meter of the turbine blade, and 90% of the total damage occurred in the first 4 m [26].

Even though there are many different designs for the lightning protection of blades, there is still potential room for improvement. On the interception of the lightning to the air terminations to increase the effectiveness of the captured lightning flashes and on the down conduction part with the connections of different parts to conduct the current safely to earth.

3.5. Blade Model for Investigation

The blade to be inspected was based on an existing model, currently the largest turbine on the market Vestas V164-9.5MW [9], at present, produced for offshore, although the company is in the process for an onshore model with similar dimensions [27]. For this study, the length of the blades was only considered for the simulation. Although their lightning protection systems are compliant with IEC 61400-24 standards, the exact lightning protection system employed by the blade's manufacturer is not available in the public domain. However, as briefly discussed in Section 3.3, any wind turbine blades should be protected and complied as per methods proposed by IEC 61400-24 standards [7]. For a structure this size, approximately with a tip height around 200 m above sea level, the number of strikes can be estimated considering the lightning density in Europe (between 0.1 and 42 flashes per year per km^2) [5,7].

The height of structure greatly affects the number of flashes predicted on the structure. Based on the regular expected turbine lifetime, what is generally predicted to be 20–25 year, it is very likely that the turbine will be hit at least once during its lifetime. Without any protection, the blade will most likely be destroyed. If the base cost lies between GBP 0.6–0.8 million per MW for an onshore turbine, and generally around 13% of these blades are [28], therefore, the estimated price for losing one blade would be roughly GBP 300,000 on the aforementioned model, not calculating the replacement, transportation,

and power outage caused costs. From this, it is clear that wind turbines require adequate protection against lightning strike nevertheless of their location, since even if it is estimated with the lowest density, over the expected lifetime the turbine will be struck at least one or two times.

4. ANSYS Workbench Implementation

4.1. ANSYS Workbench

Nowadays, engineering problems are becoming genuinely complex, relying only on theory, and. physical experiments are not practical anymore. Furthermore, deriving those with hand calculations are rather complex and time consuming. Analysis Systems (ANSYS) is one of the most reputable engineering software analysis packages available on the market and is used by many companies and research facilities around the world. The software is based on finite element analysis (FEA) to solve complex problems in single or multiphysics environment.

The basic principle of the method is that the domain or object is divided into elements with discretization. The distribution of the elements is called mesh, and the points connecting the elements are nodes. When the mesh is generated, an equation is generated for each element regarding with the solvable physics or method of analyzation. The elemental equation is than assembled to a global equation to describe the behavior of the body as a whole [29].

4.2. Blade and Protection Implementation

As briefly discussed in Sections 2 and 3, the wind turbine is a grounded structure, hence, the lightning current as a result of return stroke will then be passed safely to the ground through hub, nacelle, tower, and tower footing at the ground level. Hence, when lightning strike on the lightning receptor installed on a blade, the ground is elevated to the highest tip at the time of strike due to the blade tip being at its highest point at a time. Thus, this assumption is also used by many other lightning researchers around the world [1,3,4,8,10,14,15,19,20,26] and also for this study. Owing to that, single blade was examined without any attachment to rotor and nacelle. The ANSYS Workbench version 18.2 was used to carry out the simulation of the lightning protection of blade. The available software license was for Academic Research, which restricts the meshing node number to 300,000 which corresponds to around 40,000 elements depending on the meshing algorithm chosen. As it was mentioned earlier, the size base was taken from an existing model (Vestas V164-9.5 MW. The turbine had approximately 80 m long blades; in the model it was extended slightly to represent a potential future size. As shown in Figure 1, the hollow blade design can be seen from what was modelled in ANSYS DesignModeler. The model measurements were 85 m long, 5 m wide, 2.6 m depth, 10 times base-to-tip ratio, and 0.015 m wall thickness. The current was applied at point A, meanwhile, points B and C were specified as 0 V.
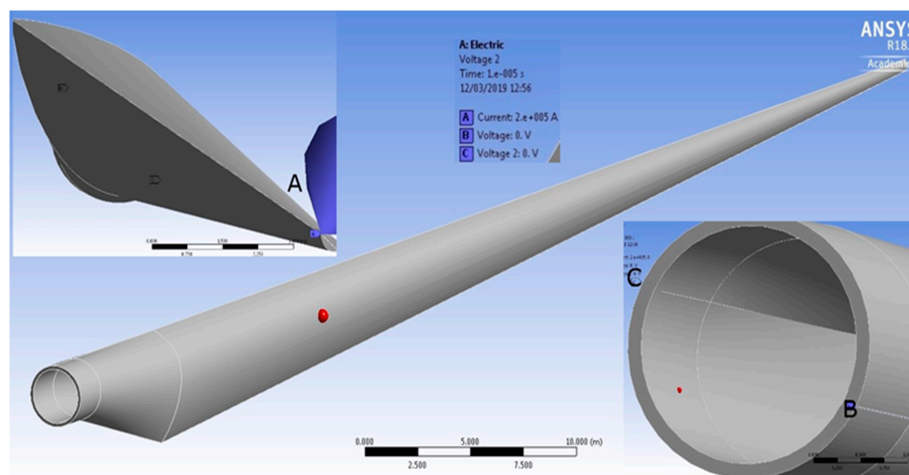

Figure 1. Wind turbine blade for simulation.

The blade material was chosen to be E-glass fiber-reinforced polyester with the necessary values set manually [30,31] to serve as an insulator-type blade, the lightning conductor was set to the copper parameters taken from standards [12] with a 50 mm^2 round cross-section as the minimal specified area. For evaluation, one of the recommended method by IEC 61400-24 [7] was considered where this method was used previously for smaller turbines, although in this project, it was examined for larger turbine blade.

4.3. Simulation Setup

For the lightning attachment point, a part on the conductor at the tip of the blade was defined (point A). In the absence of specifying ground, 0 voltage was applied on the connecting ends of the conductor (points B and C (Figure 1)).

For simulation, electric, transient-thermal, and static structural analysis was chosen using Mechanical APDL solver [32]. As shown in Figure 2, the applied mechanical APDL structure can be seen. By connecting the electric, thermal, and structural sections, it was possible to transfer results from one stage to another, creating a complex simulation environment.
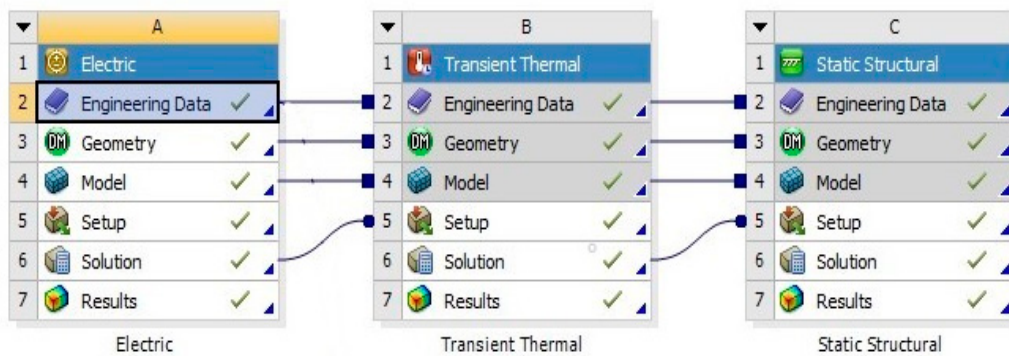

Figure 2. Simulation setup for the model.

The first and subsequent return stroke current rise were implemented according to the current standards [12], with an additional 'extreme' level of first and subsequent return stroke and the effects were observed over set amount of time as tabulated in Table 1. The 'extreme' level used referred to the highest recorded lightning peak current [2,5].

Table 1. Test parameters for simulations showing the extreme case for LPL [23].

Type of Stroke	Test Parameter	Unit	LPL
			Extreme (0)
First	Δi	kA	300
	Δt	μs	10
Subsequent	Δi	kA	75
	Δt	μs	0.25

The ambient temperature was set to 20 °C, and the blade was set to be fixed at the base. For testing the proposed method, first, the cross-section of the down conductor area was set to the recommended minimum area which was then increased to 100 mm^2 and to 200 mm^2. Afterwards, as it has been mentioned in many publications [4,26,33–35] and stated in the standards [7], lightning tends to attach to the tip and to the close approximation of the blades. Therefore, to overcome the destructive heating effect of the lightning, especially at the attachment point on the conductor, a hybrid conductor has been designed. This design consisted of two conductors with different diameters joined together. The larger diameter covered the tip of the blade and ran down at a specific distance from the tip towards

the root. The joints of the two conductors could be welded or the whole conductor could be molded to achieve a better transition between the different thicknesses. In total, six case studies were examined with different diameters and a combination of conventional and hybrid methods:

Conventional:
A: Minimal protection level with 50 mm^2 conductor cross-section area;
B: 100 mm^2 conductor cross-section area;
C: 200 mm^2 conductor cross-section area.
Hybrid:
D: Hybrid conductor design for tip;
E: Hybrid conductor design, 2 m on sides;
F: Hybrid conductor design, 5 m on sides.

The parameters examined from the simulation models were:

1. Voltage at the attachment point (V);
2. Maximum value of Joule heating in the conductor (MW/m^3);
3. Current density at the attachment point (kA/m^2);
4. Maximum temperature generated by Joule heating in the conductor (°C);
5. Total deformation caused on the blade due to the heating effect (mm);

In addition to the existing parameters, another probe was added to hybrid design at the joints of the two conductors to follow the change in the current density:

6. Current density at joint (kA/m^2).

5. Simulation Results and Discussion

5.1. Results from Conventional Case Studies

The graphical representation of the conventional design can be seen in Figure 3, where:

- Current density in the conductor;
- Temperature generated by current;
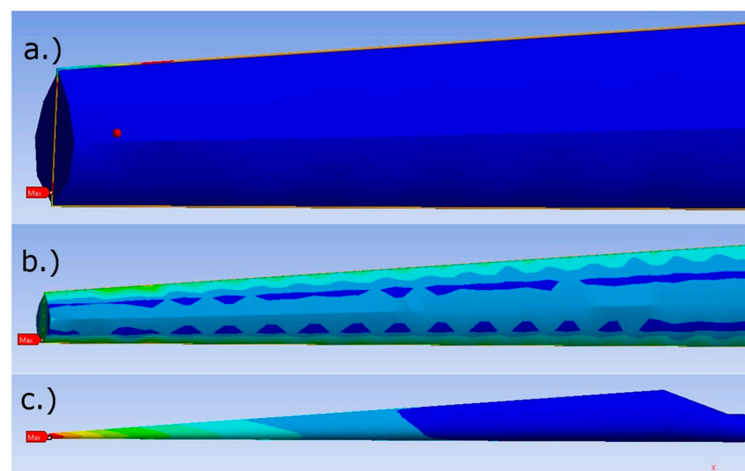- Deformation caused by temperature.

Figure 3. Graphical simulation results for conventional design; (**a**) 50 mm^2 cross section area conductor, (**b**) 100 mm^2 cross section area conductor; (**c**) 200 mm^2 cross section area conductor.

As the current from the lightning strike runs from the striking point towards ground (0 V), it heats up the conductor and the blade at the contact surfaces. Due to thermal expansion, the blade and the conductor experience force which causes deformation in both bodies.

5.1.1. Case Study A: Minimal Protection Level with 50 mm^2 Conductor Cross-Section Area

For first case, the conductor cross-section area was set to the minimal recommended 50 mm^2 value where the results of first and subsequent strokes are tabulated in Table 2. Joule heating or resistive heating occurs when electric current passing through a conductor with resistance and it is proportional to the resistance of the conductor and square of the current [36]. The maximum Joule heating occurs close to the attachment point; therefore, the maximum temperature appears at the exact same location. Thus, the highest total deformation can be seen around the tip, where the current enters the conductor.

Table 2. Results obtained from the first and subsequent return strokes for **Case Study A.**

First Strokes	LPL 0 300 kA	LPL I 200 kA	LPL II 150 kA	LPL III-IV 100 kA
Voltage at striking point (V)	4360.3	2969.9	2180.2	1453.4
Maximum joule heating (MW/m^3)	191,420	85,070	47,855	21,269
Current density at striking point (kA/m^2)	823,240	548,830	411,620	274,410
Maximum temperature (°C)	608.98	282.88	168.74	87.22
Total deformation (mm)	47.725	2.1232	1.196	5.337
Subsequent Strokes	LPL 0 75 kA	LPL I 50 kA	LPL II 37.5 kA	LPL III-IV 25 kA
Voltage at striking point (V)	1090.1	726.72	545.04	363.36
Maximum joule heating (MW/m^3)	11,964	5317.2	2991	1329.3
Current density at striking point (kA/m^2)	205,810	137,210	102,910	68,604
Maximum temperature (°C)	58.686	38.305	31.172	26.076
Total deformation (mm)	0.3019	0.13632	0.078379	0.037002

5.1.2. Case Study B: 100 mm^2 Conductor Cross-Section Area

For this case, the conductor cross-section area was increased to 100 mm^2 where the results are tabulated in Table 3 and it shown that the same parameters observed in Case Study A were decreasing as the cross-section area increases. This has been anticipated as the conductor cross-section increases, it decreases the resistance, therefore the heating and deformation as well.

Table 3. Results obtained from the first and subsequent return for **Case Study B.**

First Strokes	LPL0 300 kA	LPL I 200 kA	LPL II 150 kA	LPL III-IV 100 kA
Voltage at striking point (V)	1937.9	1292	968.97	645.98
Maximum joule heating (MW/m^3)	39,689	17,639	9922.1	4409.8
Current density at striking point (kA/m^2)	407,620	271,700	203,810	135,870
Maximum temperature (°C)	149.31	78.583	53.828	36.146
Total deformation (mm)	0.79158	0.35234	0.19862	0.08883
Subsequent Strokes	LPL 0 75 kA	LPL I 50 kA	LPL II 37.5 kA	LPL III-IV 25 kA
Voltage at striking point (V)	484.49	322.99	242.24	161.5
Maximum joule heating (MW/m^3)	2480.5	1102.5	620.13	276.1
Current density at striking point (kA/m^2)	101,900	68,936	50,952	33,968
Maximum temperature (°C)	29.957	25.536	23.989	23.081
Total deformation (mm)	0.0504	0.02311	0.01364	0.00714

5.1.3. Case Study C: 200 mm^2 Conductor Cross-Section Area

For this case, the cross-section of the lightning conductor was further increased to 200 mm^2. As was expected, the resulting values further decreased as the cross-section increased (Table 4).

Table 4. Results obtained from the first and subsequent return strokes for **Case Study C**.

First Strokes	LPL0 300 kA	LPL I 200 kA	LPL II 150 kA	LPL III-IV 100 kA
Voltage at striking point (V)	1090	726.66	545	363.33
Maximum joule heating (MW/m^3)	13,389	5950.8	3347.3	1487.7
Current density at striking point (kA/m^2)	302,270	201,510	151,130	100,760
Maximum temperature (°C)	65.017	41.118	32.754	26.78
Total deformation (mm)	0.27567	0.13922	0.079422	0.036739
Subsequent strokes	**LPL 0 75 kA**	**LPL I 50 kA**	**LPL II 37.5 kA**	**LPL III-IV 25 kA**
Voltage at striking point (V)	181.67	136.25	90.833	181.67
Maximum joule heating (MW/m^3)	371.93	209.21	92.982	371.93
Current density at striking point (kA/m^2)	50,378	37,784	25,189	50,378
Maximum temperature (°C)	23.195	23.08	23.069	23.195
Total deformation (mm)	0.01129	0.00769	0.00523	0.01129

5.2. Results from Hybrid Case Studies

Observing the previously acquired results, the conductor design was constructed to decrease the effects caused by the lightning stroke. By increasing the diameter of the conductor at the tip of the blade, should decrease the impact of the current on the body. The following three cases have been developed and examined with different length of the increased area conductor as depicted in Figure 4.
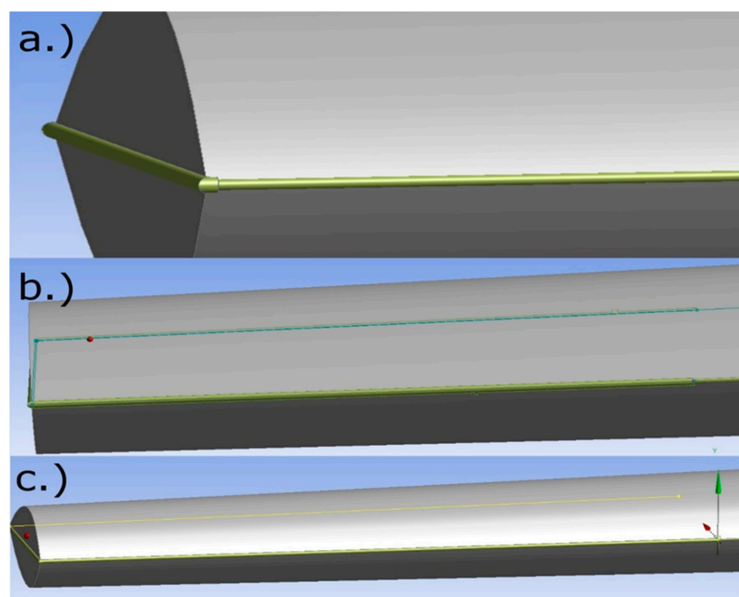

Figure 4. Hybrid conductor designs; (**a**) thicker conductor for tip, (**b**) thicker conductor for tip with 2 m on sides, (**c**) thicker conductor for tip with 5 m on sides.

5.2.1. Case Study D: Hybrid Conductor Design for Tip

In this case, the conductor cross-section area at the tip of the blade has been increased to 100 mm^2, meanwhile the rest of the conductor has been left at the minimum recommended value. Assuming that the change in diameter of the attachment area, the impact of the lightning strike attached on the conductor reduced as anticipated where results as tabulated in Table 5.

5.2.2. Case Study E: Hybrid Conductor Design, 2 m Sides

In the second case for the hybrid strategy, the length of the thicker conductor increased for 2 m on the sides of the blade, this hypothetically should further decrease the effects caused by the lightning strike. The results are tabulated in Table 6.

Table 5. Results obtained from the first and subsequent return strokes for **Case Study D.**

First Strokes	LPL0 300 kA	LPL I 200 kA	LPL II 150 kA	LPL III-IV 100 kA
Voltage at striking point (V)	4354.3	2902.8	2177.7	1451.4
Maximum joule heating (MW/m^3)	341,640	151,840	85,411	37,961
Current density at striking point (kA/m^2)	1,091,100	727,370	545,530	363,690
Maximum temperature (°C)	547.52	255.56	153.38	80.391
Total deformation (mm)	4.5937	2.043	1.502	0.5125
Current density at joints (kA/m^2)	2,715,500	1,810,400	1,357,800	905,180
Subsequent Strokes	**LPL 0 75 kA**	**LPL I 50 kA**	**LPL II 37.5 kA**	**LPL III-IV 25 kA**
Voltage at striking point (V)	1088.6	725.71	544.28	362.85
Maximum joule heating (MW/m^3)	21,353	9490.1	5338.2	2372.5
Current density at striking point (kA/m^2)	272,760	181,840	136,380	90,922
Maximum temperature (°C)	54.845	36.598	30.211	25.649
Total deformation (mm)	0.2893	0.1299	0.0741	0.0343
Current density at joints (kA/m^2)	678,890	452,590	339,440	263,000

Table 6. Results obtained from the first and subsequent return strokes for **Case Study E.**

First Strokes	LPL0 300 kA	LPL I 200 kA	LPL II 150 kA	LPL III-IV 100 kA
Voltage at striking point (V)	2773.4	1848.9	1386.7	924.45
Maximum joule heating (MW/m^3)	66,067	29,363	16,517	7340.8
Current density at striking point (kA/m^2)	844,930	563,290	422,470	281,640
Maximum temperature (°C)	237.15	117.62	75.788	45.906
Total deformation (mm)	1.355	0.6034	0.3404	0.1525
Current density at joints (kA/m^2)	2,072,100	1,381,400	1,036,100	690,700
Subsequent Strokes	**LPL 0 75 kA**	**LPL I 50 kA**	**LPL II 37.5 kA**	**LPL III-IV 25 kA**
Voltage at striking point (V)	693.34	462.23	346.67	23.11
Maximum joule heating (MW/m^3)	4129.2	1631.3	1032.3	458.8
Current density at striking point (kA/m^2)	211,230	140,820	105,620	70,411
Maximum temperature (°C)	35.447	27.978	25.362	23.494
Total deformation (mm)	0.0867	0.0398	0.0234	0.0118
Current density at joints (kA/m^2)	518,030	345,350	259,010	172,680

5.2.3. Case Study F: Hybrid Conductor Design, 5 m Sides

The thicker portion of the conductor has been further increased to 5 m on each side of the tip of the blade, in theory, further reducing the recorded values where results are tabulated in Table 7.

Table 7. Results obtained from the first and subsequent return strokes for **Case Study F.**

First Strokes	LPL0 300 kA	LPL I 200 kA	LPL II 150 kA	LPL III-IV 100 kA
Voltage at striking point (V)	2691.2	1794.1	1345.6	897.06
Maximum joule heating (MW/m^3)	64,236	28,549	16,059	7137.3
Current density at striking point (kA/m^2)	495,610	330,410	247,800	165,200
Maximum temperature (°C)	218.42	115.85	74.788	45.461
Total deformation (mm)	1.216	0.5420	0.3061	0.1376
Current density at joints (kA/m^2)	1,999,800	1,333,200	999,910	666,610
Subsequent Strokes	**LPL 0 75 kA**	**LPL I 50 kA**	**LPL II 37.5 kA**	**LPL III-IV 25 kA**
Voltage at striking point (V)	672.8	488.53	336.4	224.27
Maximum joule heating (MW/m^3)	4014.7	1784.3	1003.7	446.08
Current density at striking point (kA/m^2)	123,900	82,601	61,951	41,301
Maximum temperature (°C)	35.197	27.865	25.299	23.466
Total deformation (mm)	0.0787	0.0366	0.0218	0.0114
Current density at joints (kA/m^2)	499,960	333,300	249,980	166,650

5.3. Discussion

5.3.1. Conventional Cases (A, B, and C)

Based on the simulation results on the conventional type conductor tabulated in Tables 2–4, the current density at the attachment point and total deformation (highest value at the tip of the blade) plot can be seen on Figure 5. Comparing the graphs, it can be seen that increasing the diameter of the conductor reduces the value of current density and the amount of deformation produced on the blade as it can be expected. Although, further inspecting the results, the difference between the 100 mm^2 and the 200 mm^2 cross-section area was less significant (34.8%) than the difference between the 50 mm^2 and 100 mm^2 (101.9%). Increasing the diameter of the conductor implied better results or lower values, although it was not linear compared to the change in diameter. Evaluating the results leads to the assumption that the 100 mm^2 cross-section area produced the best results among the tested values according to the given LPL, considering the weight and cost of the usable material. Similar correlations can be seen on the graphs from the rest of the results in Figure A1 (Appendix A).
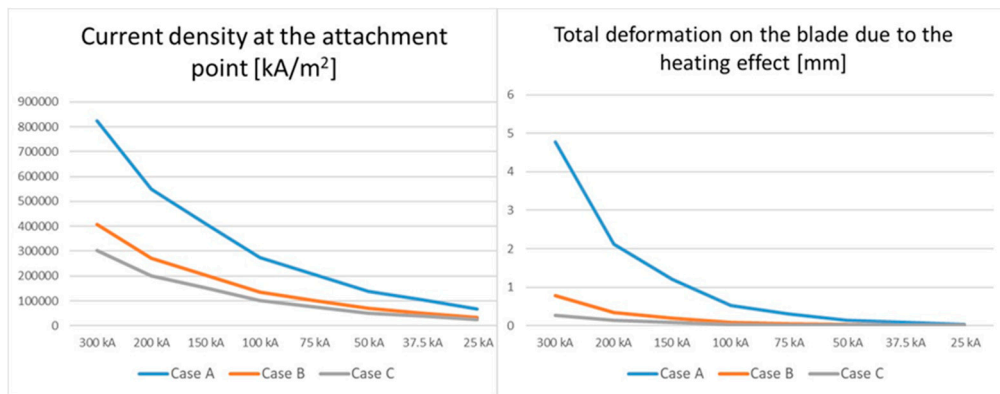
Figure 5. Current density (**left**) and total deformation of the blade (**right**) for the conventional case studies.

5.3.2. Hybrid Cases (D, E, and F)

As shown in Figure 6, the graphical representation of the simulation results can be seen for Case E.
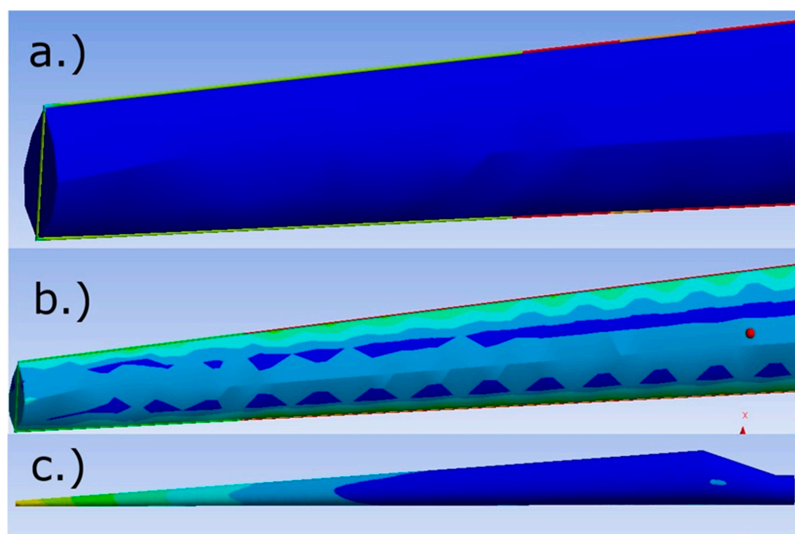

Figure 6. Graphical simulation results, hybrid design (case study E); (**a**) current density in the conductor, (**b**) temperature generated by current, (**c**) deformation caused by temperature.

Based on the data tabulated in Tables 5–7, Figure 7 plotted the different current densities at different points comparing three different hybrid cases. When diameters increased, the current density reduced in the conductor as well as heating and deformation in the blade. On the other hand, at the joints of the two types of conductor, there was still an increment that could still be seen. Comparing the values of the three designs indicates that the tip only version reduces the effects of the stroke at the attachment point the least, although increasing the length of the higher diameter conductor reduces the current density at both the attachment point and at joint. The increase in current density between the attachment point and the joint, for case D, case E, and case F with 148.9%, 145.2%, and 303.5%, respectively, thus the possible damage due to the current flowing in the down conductors. This suggests that the most efficient way to improve the LPS would be to increase the overall diameter of the whole conductor.
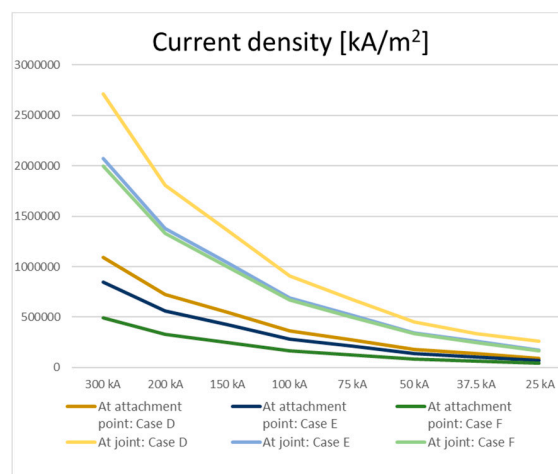
Figure 7. Current density of hybrid case studies.

As shown in Figure 8, on the left, the maximum temperature of the blade, which was measured at conductor joints and on the right the total deformation caused on the blade, where the highest measured value was at the tip of the blade. It shows that there was no significant reduction in temperature and deformation between the 2 m and 5 m type (8% for temperature and 11.4% for deformation), although, the maximum temperature point moved from the area of attachment point to the joints of the two conductor. Comparing the three tested designs' results, the 2 m long conductor is suggested to be the most sufficient of all, considering the amount of material involved and the improvement in temperature, thus reduction in deformation too. The rest of the results can be seen in Figure A2.
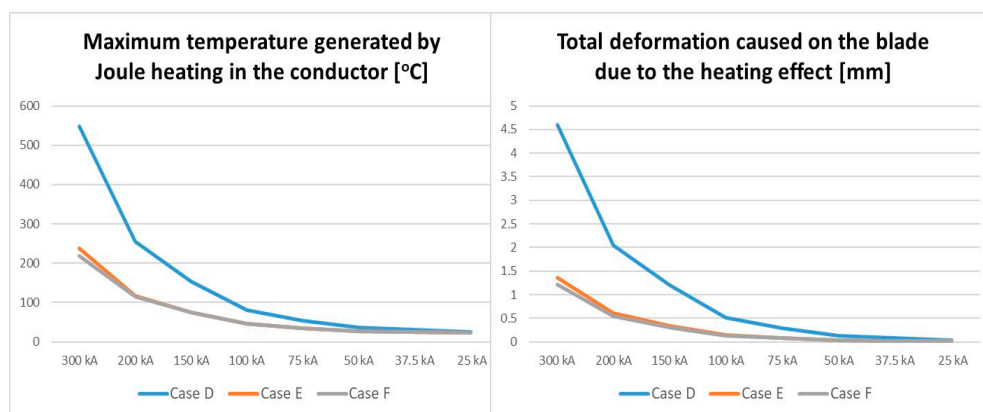

Figure 8. Maximum temperature (**left**) and total deformation of the blade (**right**) for the hybrid case studies.

5.3.3. Conventional and Hybrid

As shown in Figure 9, on the left, the maximum temperature of the blade, meanwhile on the right, the total deformation caused on the blade, where the highest measured value was at the tip of the blade. It can be seen that both the B and E cases performed better compared to the minimal conductor cross-section area in terms of temperature increment and blade deformation. For LPL 0, the temperature difference between Case B and A was 459.67 °C (307.86%), meanwhile between Case E and A it was 371.83 °C (156.79%), furthermore, the temperature difference between Case B and E is 87.74 °C. Furthermore, the temperature increase is linearly proportional to the deformation and the changes for deformation are nearly identical.
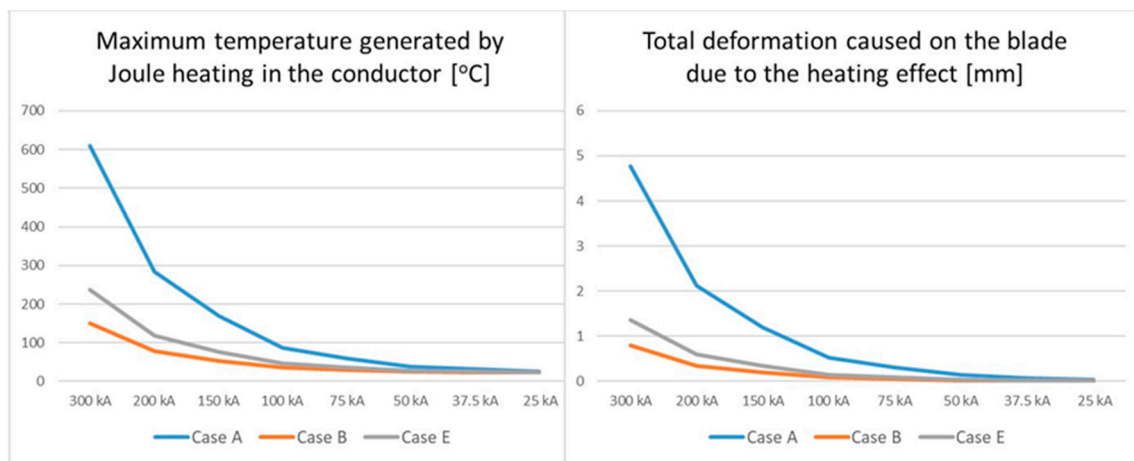
Figure 9. Maximum temperature (**left**) and total deformation (**right**) of the blade at A, B, and E case studies.

Comparing Cases B and E, the results showed that Case B suggests the most effective conductor design in terms of temperature and displacement, also the other measured parameters.

5.3.4. Summary

Comparing results obtained from Case Studies, it can be deduced that the most efficient way of increasing the efficiency of the protection of a wind turbine blade is to increase the diameter of the down conductor. However, it will be compromised due to the actual cost of the extra material, the weight increasement and the possible effects on the airfoil of the blades as these factors are the most crucial in blade design. Furthermore, applying Case E to a modern turbine blade could potentially reduce the effects of the heat and deformation because it only requires small portion of the conductor in the tip region. In general, most turbines are glued together at the leading and trailing edge to reduce the manufacturing costs, this brings an issue since the down conductors placed along these lines. As the current heats up the conductor, this could possibly melt the applied glue material causing severe damage which may cause blade to separate. As to potentially alleviate this, it would be possible to implement the hybrid conductor design for the blade lightning protection.

6. Conclusions, Recommendations for Future Works

6.1. Conclusions

Lightning protection is an important aspect of wind energy, since over the expected lifetime of a turbine; at least once a lightning will hit it. Due to the enormous amount of current, without proper protection, it is most likely to result failure to turbine and will cause high repair costs. The protection methods and levels are proposed by standards to achieve the minimal protection suggested, although this protection cannot be taken as guarantee for all cases. As wind turbines keep increase in size to

keep up with the generation demand, as the chance increases, of being hit by a lightning due to their elevation from ground level.

In this paper, a conventional lightning protection concept, previously used for smaller turbine models has been evaluated for possible use for large blades. For the task, simulation software, ANSYS Workbench, Mechanical APDL has been used. In the first three case studies, different conductor cross-section areas have been set for conventional design for full length of the conductor. For the second half of the case studies a hybrid conductor model was evaluated. This design consists of two conductors with different diameters joined together. The higher diameter one covered the tip of the blade and ran down at specific distance from the tip towards the root. The lightning parameters was set according to the current standards, with and additional extreme first and subsequent return stroke current amplitude. Comparing the simulation outcomes has been showed that Case Study C indicated the most promising results among all. In the other hand considering the weight and cost of the extra material, also the possible aerodynamical effects of the conductor around the blade, Case Study E has been appeared to be the most adequate alternative. The design shows great improvement in reducing the lightning caused effects, compared to Case Study A, therefore the possible damage on the blade. Furthermore, it only requires simple modification of the existing lightning protection concept, minimizing the associated costs, weight, and the possible disturbance in the aerodynamics of the blade.

6.2. Recommendations for Future Work

There are still many factors and values that should be evaluated in order to give full understanding and clarification of the proposed design.

- One possible future work could include the examination of electromagnetic forces and waves generated by the current, since those were excluded from the simulation due to missing Mechanical APDL functions (electromagnetic analysis system).
- There are possible incorrect, unrealistic values presented in this work due to the potential misconfiguration of simulation physics in the absence of relatable guide.
- The software used had limited solver size due to academic license; therefore, the mesh of the objects had to be left coarse, meaning less accurate and possible differences in expected and real life values.
- The design and therefore the investigation could be extended to model a complete turbine to see the effects on the whole structure.
- The exact length of the increased diameter conductor could be evaluated in the ratio of the size of the blade; therefore, the proposed design could be implemented on various size blades with maximum efficiency.
- A comparison could be made with existing blade LPS what is used on large blades nowadays to estimate the efficiency of both designs.
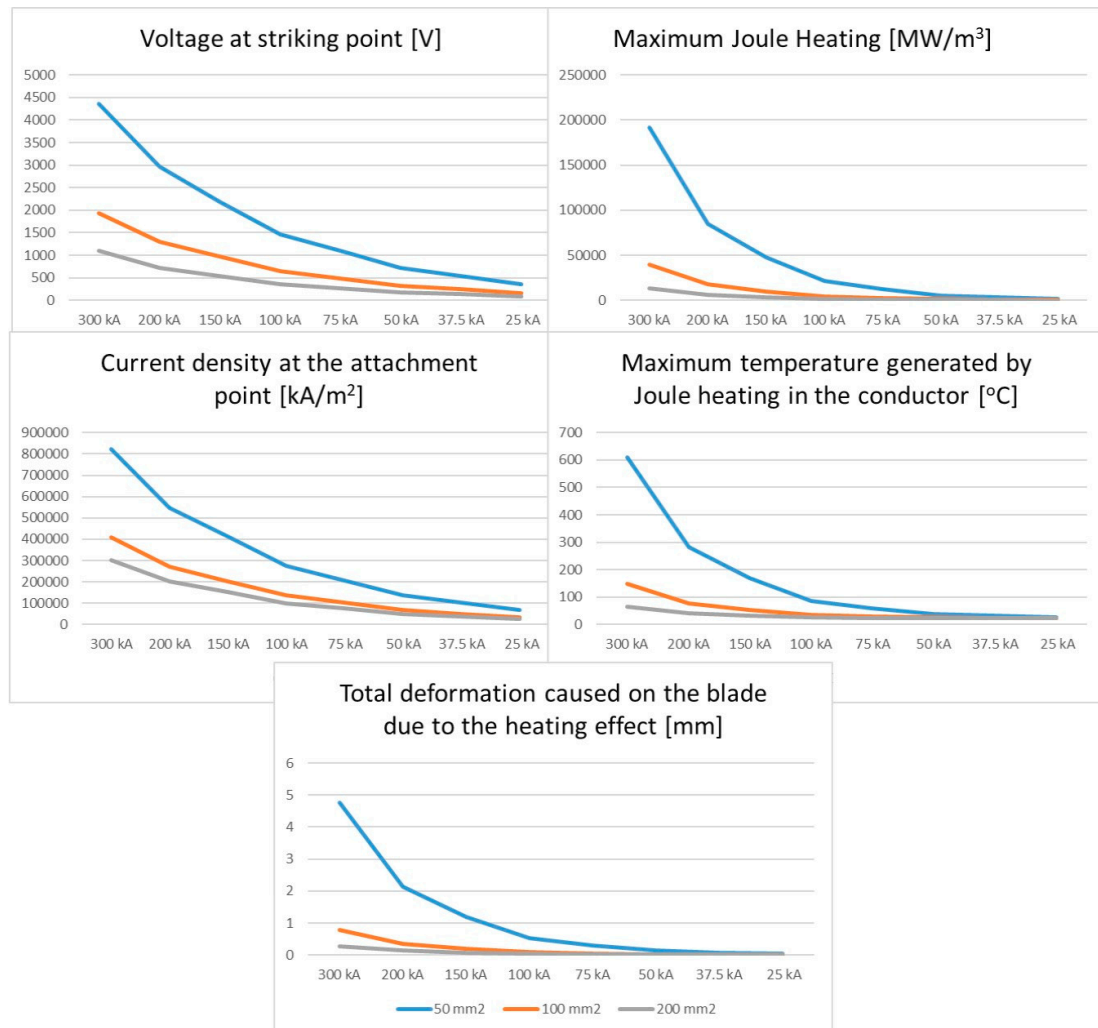
Appendix A

Figure A1. Plotted results from conventional simulations.
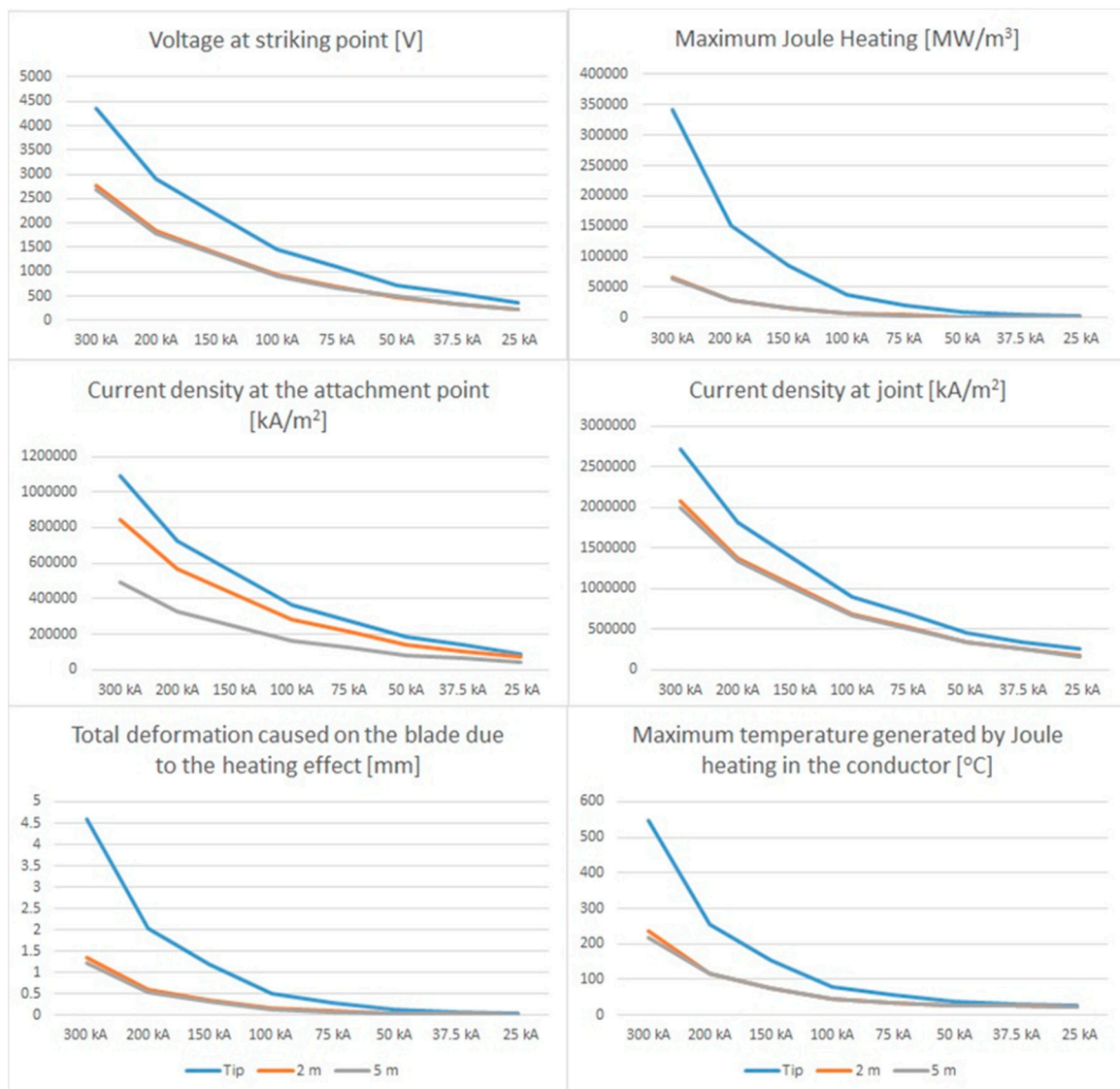
Figure A2. Plotted results from hybrid simulations.

References

1. Cooray, V. *An Introduction to Lightning*; Springer: Heidelberg, Germany, 2015.
2. NSSDC. Sun Fact Sheet. Available online: https://nssdc.gsfc.nasa.gov/planetary/factsheet/sunfact.html (accessed on 2 October 2018).
3. Rakov, V.A.; Uman, M.A. *Lightning: Physics and Effects*; Cambridge University Press: Cambridge, UK, 2003.
4. Cooray, V. *Lightning Protection*; The Institution of Engineering and Technology: London, UK, 2010.
5. The Weather Channel. Where Almost 9 Billion Lightning Strikes in 5 Years Have Happened on Earth. Available online: https://weather.com/safety/thunderstorms/news/2018-05-07-world-lightning-strikes-map-vaisala-2013-2017 (accessed on 2 February 2019).
6. Anderson, G.; Klugmann, D. European lightning density analysis using 5 years of ATDnet data. *Nat. Hazards Earth Syst. Sci.* **2014**, *14*, 815–829. [CrossRef]
7. Technical Committee PEL/88. *Wind Turbines Part. 24: Lightning Protection, BS EN 61400-24:2019*; The British Standards Institution: London, UK, 2019.
8. Uman, M.A. *The Lightning Discharge*; Dover Publications, Inc.: Mineola, NY, USA, 2001.

9.   HMI Vestas Offshore Wind. The World's Most Powerful Available Wind Turbine Gets Major Power Boost. Available online: http://www.mhivestasoffshore.com/worlds-most-powerful-available-wind-turbine-gets-major-power-boost/ (accessed on 5 February 2019).

10. Hu, W. *Advanced Turbine Wind Technology*; Springer: Ithaca, NY, USA, 2018.

11. Czeshop. Wind Turbine Blade Cross Section. Available online: http://czeshop.info/2017/wind-turbine-blade-cross-section.html (accessed on 10 February 2019).

12. Technical Committee GEL/81. *Protection against Lightning Part. 1: General Principles, BS EN 62305-1:2011*; The British Standards Institution: London, UK, 2017.

13. Cooray, V. *Lightning Protection*; Athenaeum Press Ltd.: Gateshead, UK, 2010.

14. Barwise, A. Lightning and Surge Protection for Wind Turbines. Available online: https://www.ee.co.za/article/lightning-surge-protection-wind-turbines-2.html (accessed on 21 February 2019).

15. Wilson, N.; Myers, J.; Cummins, K.L.; Hutchinson, M.; Nag, A. Lightning attachment to wind turbines in Central Kansas: Video observations, correlation with the NLDN and in-situ peak current measurements. In Proceedings of the European Wind Energy Conference Exhibition EWEC 2013, Vienna, Austria, 4–7 February 2013.

16. Cummins, K.L.; Zhang, D.; Quick, M.G.; Garolera, A.C.; Myers, J. Overview of the Kansas Windfarm2013 Field Program. In Proceedings of the 23rd International Lightning Detection Conference (ILDC), Tucson, AZ, USA, 18–19 March 2014.

17. Wang, D.; Takagi, N.; Watanabe, T.; Sakurano, H.; Hashimoto, M. Observed characteristics of upward leaders that are initiated from a windmill and its lighting protection tower. *Geophys. Res. Lett.* **2008**, *35*. [CrossRef]

18. Ishii, M.; Saito, M.; Natsuno, D.; Sugita, A. Lighting current observed at wind turbines at winter in Japan. In Proceedings of the International Conference on Lightning & Static Electricity ICLOSE 2013, Seattle, WA, USA, 18–20 September 2013.

19. Yasuda, Y.; Yokoyama, S.; Minowa, M. Classification of Lightning Damage to Wind Turbine Blades. *IEEJ Trans. Electr. Electr. Eng.* **2012**, *7*, 559–566. [CrossRef]

20. Sorensen, T.; Jensen, F.V.; Raben, N. Lightning protection for offshore wind turbines. In Proceedings of the 16th International Conference & Exhibition on Electricity Distribution, Amsterdam, The Netherlands, 18–21 June 2001.

21. Solacity. Lightning Protection. Available online: https://www.solacity.com/lightning-protection/ (accessed on 30 March 2019).

22. Yasuda, Y.; Yokoyama, S. Proposal of Lightning Damage Classification to Wind Turbine Blades. In Proceedings of the 7th Asia Pacific International Conference on Lightning (APL), Chengdu, China, 1–4 November 2011; pp. 368–371.

23. GlobalBladeService. Lightning Damage. Available online: https://www.globalbladeservice.eu/blade-service/lightning-damage (accessed on 31 March 2019).

24. Gorgeouswithattitude. 1st Blade Wends Way to Wind Farm. Available online: http://gorgeouswithattitude.blogspot.com/2010/09/1st-blade-wends-way-to-wind-farm.html (accessed on 31 March 2019).

25. EPSRC, Lightning Protection of Wind Turbine. Available online: https://community.dur.ac.uk/supergen.wind/docs/presentations/2010-04-25_1425_EWEC%202010_SideEvent_Lightning_VP.pdf (accessed on 31 March 2019).

26. Garolera, A.C.; Madsen, S.F.; Nissim, M.; Myers, J.D.; Holboell, J. Lightning Damage to Wind Turbine Blades From Wind Farms in the U.S. *IEEE Trans. Power Deliv.* **2016**, *31*, 1043–1049. [CrossRef]

27. MHI Vestas Offshore Wind A/S. V164-9.5 MW. Available online: http://www.mhivestasoffshore.com/category/v164-9-5-mw/ (accessed on 24 February 2019).

28. Schubel, P.J. Technical cost modelling for a generic 45-m wind turbine blade producedby vacuum infusion (VI). *Renew. Energy* **2010**, *35*, 183–189. [CrossRef]

29. Alawadhi, E.M. *Finite Element Simulations Using ANSYS*, 2nd ed.; CRC Press: Boca Raton, FL, USA, 2015.

30. AZoNetwork. E-Glass Fibre. Available online: https://www.azom.com/properties.aspx?ArticleID=764 (accessed on 25 February 2019).

31. MatWeb. Glass Fiber Summary List. Available online: http://www.matweb.com/search/DataSheet.aspx?MatGUID=5c6df0ae272e41808562d3374d7b4f5a&ckck=1 (accessed on 28 February 2019).

32. ANSYS, Inc. Analysis Types. Available online: https://www.sharcnet.ca/Software/Ansys/18.2.2/en-us/help/wb_sim/ds_simulation_types.html (accessed on 2 March 2019).

33. Heidler, F.; Flisowski, Z.; Zischank, W.; Bouquegneau, C. Parameters of lightning current given in IEC 62305–Background, experience and outlook. In Proceedings of the 29th International Conference on Lightning Protection ICLP 2008, Uppsala, Sweden, 23–26 June 2008.

34. Guo, Z.; Li, Q.; Ma, Y. Experimental study on lightning attachment manner to wind turbine blades with lightning protection system. *IEEE Trans. Plasma Sci.* **2019**, *47*, 635–646. [CrossRef]

35. Arif, W.; Li, Q.; Guo, Z.; Ellahi, M.; Wang, G.; Siew, W.H. Experimental study on lightning discharge attachment to the modern wind turbine blade with lightning protection system. In Proceedings of the 13th International Conference on Emerging Technologies (ICET), Islamabad, Pakistan, 27–28 December 2017; pp. 1–6.

36. Young, J.H. Steady state Joule heating with temperature dependent conductivities. *Appl. Sci. Res.* **1986**, *43*, 55–65. [CrossRef]